

# Spectroscopy of Brown Dwarf Candidates in the $\rho$ Ophiuchi Molecular Core <sup>1</sup>

Bruce A. Wilking <sup>2</sup>

Department of Physics and Astronomy, University of Missouri-St. Louis  
 8001 Natural Bridge Road, St. Louis, MO 63121  
 brucew@newton.umsl.edu

Thomas P. Greene <sup>2</sup>

Lockheed Martin Missiles & Space, 3251 Hanover St.  
 Palo Alto, CA 94304-1191  
 tgreene@meer.net

and

Michael R. Meyer <sup>3</sup>

Steward Observatory, The University of Arizona, Tucson, AZ 85721  
 mmeyer@gould.as.arizona.edu

## ABSTRACT

We present an analysis of low resolution infrared spectra for 20 brown dwarf candidates in the core of the  $\rho$  Ophiuchi molecular cloud. Fifteen of the sources display absorption-line spectra characteristic of late-type stars. By comparing the depths of water vapor absorption bands in our candidate objects with a grid of M dwarf standards, we derive spectral types which are independent of reddening. Optical spectroscopy of one brown dwarf candidate confirms the spectral type derived from the water bands. Combining their spectral types with published near-infrared photometry, effective temperatures and bolometric stellar luminosities are derived enabling us to place our sample on the Hertzsprung-Russell diagram. We compare the positions of the brown dwarf candidates in this diagram with two sets of theoretical models in order

---

<sup>1</sup>Observations reported in this study were obtained at the Multiple Mirror Telescope Observatory, a facility operated jointly by the Smithsonian Institution and the University of Arizona.

<sup>2</sup>Visiting Astronomer at the Infrared Telescope Facility, which is operated by the University of Hawaii under contract from the National Aeronautics and Space Administration.

<sup>3</sup>Hubble Fellow

to estimate their masses and ages. Considering uncertainties in placing the candidates in the H-R diagram, six objects consistently lie in the brown dwarf regime and another five objects lie in the transition region between stellar and substellar objects. The ages inferred for the sample are consistent with those derived for higher mass association members. Three of the newly identified brown dwarfs display infrared excesses at  $\lambda=2.2\text{ }\mu\text{m}$  suggesting that young brown dwarfs can have active accretion disks. Comparing our mass estimates of the brown dwarf candidates with those derived from photometric data alone suggests that spectroscopy is an essential component of investigations of the mass functions of young clusters.

*Subject headings:* stars: pre-main-sequence, brown dwarfs – infrared: stars – ISM: individual ( $\rho$  Ophiuchi cloud)

## 1. Introduction

The shape of a star cluster's Initial Mass Function (IMF) at and below the hydrogen burning limit can yield important information about the star formation process as well as the relative importance of brown dwarfs in a localized region of the Galaxy. It is becoming evident that in most clusters, the IMF below  $0.3\text{ M}_\odot$  is approximately flat in logarithmic mass units and that the total cluster mass is not dominated by the lowest mass members (see Luhman *et al.* 1998 and references therein). Yet the detailed shape of the IMF in clusters below  $0.3\text{ M}_\odot$  is poorly defined (see Scalo 1998 for review). To constrain the slope of a cluster IMF in this mass range, it will be necessary to identify significant numbers of brown dwarfs. This is most easily accomplished in young clusters since low mass objects are most luminous in their youth. As demonstrated in models by Burrows *et al.* (1997), deuterium burning stabilizes the luminosity of a contracting brown dwarf such that its luminosity at  $10^6$  years is about 3 orders of magnitude greater than at  $10^9$  years. Recent visible wavelength studies of the Orion Nebula Cluster (ONC, Hillenbrand 1997) and the Taurus molecular cloud (Briceño *et al.* 1998) have indeed been successful in detecting several young, substellar mass objects. But due to their cool effective temperatures ( $<3000\text{ K}$ ) and the large columns of dust in regions of star formation, young brown dwarfs are most easily observed at near-infrared wavelengths. Models predict that in the closest star-forming regions ( $d\approx150\text{ pc}$ ), pre-main sequence (PMS) stars of age  $10^6$  years at the hydrogen-burning limit will have apparent magnitudes of  $K\text{ }(2.2\text{ }\mu\text{m})=15.5^m$  when viewed through  $A_v=50^m$  and will be easily detectable in deep ground-based near-IR surveys.

The  $\rho$  Ophiuchi molecular cloud lies in the Upper Scorpius subgroup of the Sco-Cen OB association. At a distance of only 150 pc (de Zeeuw *et al.* 1997), it is an ideal area to search for young brown dwarfs. It is the highest stellar density region of low mass star formation among clouds within 200 pc of the Sun. It hosts over 100 young stellar objects (YSOs) in its  $1\text{ pc} \times 2\text{ pc}$  centrally condensed core (Grasdalen, Strom, & Strom 1973; Vrba *et al.* 1975; Wilking & Lada 1983; Greene & Young 1992; Comerón *et al.* 1993; Strom, Kepner & Strom 1995). The central regions of the core, with  $A_v$  estimated to be  $50^m$ – $100^m$ , provide an effective screen of background stars even at infrared wavelengths. The PMS stars in the core have an estimated age of  $<10^6$  years (Greene & Meyer 1995) and theoretical models predict that brown dwarfs of this age and distance will be easily detected at near-infrared wavelengths over a broad range of masses. Previous infrared studies in the  $\rho$  Oph core have used broadband photometry to estimate masses of YSOs and identify substellar candidates (e.g., Rieke & Rieke 1990; Comerón *et al.* 1993; Strom, Kepner & Strom; Williams *et al.* 1995; Comerón, Rieke & Rieke 1998). Comerón and collaborators have gone a step farther and derived an IMF for this cluster which is relatively flat down to  $0.05\text{ M}_\odot$  (Comerón, Rieke, & Rieke 1996). Yet this result depends on large completeness corrections at the lowest masses and, in most cases, the mass estimates have not been confirmed by spectroscopy. Using optical spectroscopy, Luhman *et al.* (1997) have confirmed one of the candidates, 162349.8-242601, as a brown dwarf with a mass of  $0.01$ – $0.06\text{ M}_\odot$ .

In this contribution, we use low resolution infrared spectroscopy in the  $\lambda=2.2\text{ }\mu\text{m}$  window to identify substellar objects in the core of the  $\rho$  Oph cloud. The infrared spectral region is necessary since brown dwarf candidates in this cloud will be obscured by dust, and a spectral resolution of  $R \sim 300$  is adequate given the very broad nature of molecular features in cool objects. In Section 2, we describe our selection of brown dwarf candidates using published near-infrared photometry. A description of how the infrared spectra were obtained for 20  $\rho$  Oph brown dwarf candidates and 14 late-type dwarf standards is also given in Section 2. Section 3 introduces a new technique, calibrated with a grid of M dwarf standards, that uses water vapor absorption bands in the infrared spectra to derive spectral types. As a result, 15 brown dwarf candidates are assigned late-type spectral classifications, with ten objects classified as M6 or later. The spectral classification for one PMS star is confirmed through optical spectroscopy. Given their spectral types, the effective temperatures and bolometric luminosities of the brown dwarf candidates are estimated in Section 4. Using a Hertzsprung-Russell diagram and two sets of pre-main-sequence tracks, we find that 6 candidates clearly fall in the brown dwarf regime and 5 candidates lie in the stellar/substellar transition region. Section 5 presents a discussion of the infrared excesses of the probable brown dwarfs and compares our mass estimates with those from infrared photometric studies.

## 2. Observations & Source Selection

Low resolution infrared spectra were obtained for 14 late-type dwarf spectral standards and 20 objects in the core of the  $\rho$  Ophiuchi molecular cloud. Logs of the Ophiuchus observations are given in Table 1. Included for each program object is the date of observation, the total on-source integration time, and the reference star used to divide out telluric features. In addition, one  $\rho$  Oph object, GY 5, was observed with the MMT Red Spectrograph. All observations are described in more detail in the sections below.

### 2.1. Sample Selection

Most of the 20 brown dwarf candidates in the core of the  $\rho$  Oph cloud observed spectroscopically were selected from the two-micron survey of Comerón *et al.* (1993). Not only is the magnitude limit of their survey comparable to the detection limit for our spectroscopic observations ( $K < 14.5^m$ ), but they concentrated on the highest extinction region of the cloud core where  $A_v = 50\text{--}100^m$  and contamination by background stars is minimal. We supplemented the Comerón *et al.* sample with sources from the near-infrared survey of Greene & Young (1992) and an unpublished near-infrared survey of  $\rho$  Oph Core A by this group. Candidates were chosen on the basis of their estimated absolute K magnitudes with  $M(K) \geq 3$ <sup>4</sup>. In other words, we preferentially selected sources which were faint at K and had values of  $(H - K) \leq 2$ . The small  $(H - K)$  colors favor PMS stars near the surface of the cloud and/or with small infrared excesses which minimizes the effects of spectral veiling.

A  $K$  vs.  $(H - K)$  diagram for the 20 brown dwarf candidates is shown in Fig. 1 relative to the zero-age main sequence and a  $3 \times 10^5$  year old isochrone. The median values of apparent K magnitude,  $(H - K)$  color, and absolute K magnitude for our 20 objects are  $K = 12.4^m$ ,  $(H - K) = 1.3^m$ , and  $M(K) = 4.5^m$ . Among the 14 objects in the Comerón *et al.* survey with  $K < 14^m$  and  $M(K) > 4^m$ , we obtained infrared spectra for ten. Our selection criteria appear to have been successful at picking PMS stars in the cloud, and only 3 objects are suspected background stars (Sec. 3.3). The heavily reddened source GY 31 was

---

<sup>4</sup>The absolute K magnitude,  $M(K)$ , was estimated using the standard formula  $M(K) = m(K) - A(K) - DM$  where  $m(K)$  is the apparent K magnitude,  $A(K)$  is the extinction at K, and  $DM = 5.9^m$  which is appropriate for the Ophiuchus cloud. The extinction at K was estimated from  $A(K) = 1.4 \times E(H - K)$  (Cohen *et al.* 1981) assuming an intrinsic  $(H - K)_0 = 0.3$  typical for an M dwarf and no infrared excess. For comparison, a PMS star of age  $3 \times 10^5$  years and  $M = 0.10 M_\odot$  is predicted to have a  $M(K) = 4.2$  (D'Antona & Mazzitelli 1998).

observed unintentionally, as it fell into the slit during an attempt to observe GY 30.

## 2.2. IRTF Grism Observations

All infrared spectra were obtained between 1996 June and 1998 January with the 3.0 m NASA IRTF on Mauna Kea. Observations were made using the facility infrared camera, NSFCAM, in the K band with the HKL grism, a 0.3 arcsec pixel<sup>−1</sup> scale, and a 0.6'' slit (see Shure *et al.* 1994 and Rayner *et al.* 1998 for a description of the instrument and grism). The spectra cover the 2.0–2.5  $\mu\text{m}$  band and have a resolution  $R=\lambda/\Delta\lambda \sim 300$ . Flat field exposures of the dome interior illuminated with incandescent lamps were taken at the beginning of each night. A typical set of observations consisted of the star observed at two positions along the slit, separated by 10 arcsec. Typical exposure times for the brown dwarf candidates were 120–180 seconds per slit position and limited by variations in the atmospheric OH emission. Total on-source integration times were typically 2 minutes for the standard star observations (but extended for 9 minutes for the M9 stars) and 18 minutes for the brown dwarf candidates (see Table 1). Before extraction, the spectral images in each set were sky-subtracted using their companion image, and divided by a flat-field. Wavelength calibration was established using OH emission lines. After extraction, telluric features in the spectra were removed by dividing by the spectrum of a dwarf star near spectral type A0 and observed typically within 30–40 minutes and within 0.1 airmasses of the program objects. The airmass difference between the telluric standard and program star never exceeded 0.25. No attempt was made to restore the true continuum shape of the program objects; to recover the true shape one could multiply each spectrum by a blackbody corresponding to the effective temperature of the telluric standard. Because of the steep response function of the grism, it was not possible to extrapolate over the Br  $\gamma$  absorption line in the telluric standard and hence we were not sensitive to Br  $\gamma$  emission in the program stars. The telluric standard star used for each brown dwarf candidate is listed, along with their spectral types, in the last column of Table 1.

## 2.3. MMT Red Spectrograph

A low resolution optical spectrum was obtained for GY 5 under non-ideal conditions on 1998 February 13, at the Multiple Mirror Telescope on Mt. Hopkins. We used the Red Channel spectrograph with the 270 line mm<sup>−1</sup> grating and a 2'' wide slit resulting in a resolution of 23.5 Å per spectral element over the range 6500–9500 Å. The detector was a 1200  $\times$  800 pixel Loral CCD which was binned  $\times 2$  in the spatial dimension. Data

were taken in beam-switching mode, nodding the source along the slit with integration times of 600 seconds per exposure. Image processing was accomplished by subtracting beam-switched pairs from each other to remove bias, dark current and sky emission. The subtracted frames were flat-fielded and corrected for grating efficiency using a set of calibration frames obtained with a featureless quartz lamp. Wavelength calibration was achieved with a comparison spectrum taken with a HeNeAr lamp. The individual spectra were then extracted and the local sky level was re-calculated using apertures adjacent to that containing the source spectrum. The four spectra were median filtered, and the resultant spectrum was smoothed with a gaussian of half-width  $\sigma = 11.5\text{\AA}$  for comparison with the library of spectral standards from Kirkpatrick, Henry, & McCarthy (1991).

### 3. Results

Infrared spectra of 13 standard stars, ranging in spectral type from K5V to M9V, are shown in Fig. 2 with the most prominent atomic and molecular absorption features labeled. Spectral classifications were adopted from Kirkpatrick, Henry, & McCarthy (1991) or Henry, Kirkpatrick, & Simons (1994). Also shown is a spectrum of the star BRI 0021-0214 which has tentatively been classified as  $>\text{M9.5V}$  (Kirkpatrick, Beichman, & Skrutskie 1997). Apparent in the dwarf spectra are narrow absorption lines by Na I (blended doublet at  $2.21\text{ }\mu\text{m}$ ), Ca I (blended triplet at  $2.26\text{ }\mu\text{m}$ ), and the CO  $\Delta\nu=2$  bands ( $2.29\text{--}2.42\text{ }\mu\text{m}$ ). Not labeled are broad absorptions by H<sub>2</sub>O vapor at the beginning and end of the bandpass. Sections of the spectra have been removed that span the wavelengths of the Br $\gamma$  absorption line ( $2.166\text{ }\mu\text{m}$ ) in the telluric standard, and where division of atmospheric features was poor ( $\sim 2.03\text{ }\mu\text{m}$ ). ASCII data files of the 14 standard star spectra and a table of the observational details are electronically available upon request.

#### 3.1. Spectral Classifications Using Water Vapor

At this low spectral resolution, there are no absorption lines present in our spectra that can be reliably used to derive spectral types. However, the depths of the broad water vapor absorption bands are extremely sensitive to spectral type for M dwarfs. We have derived a quantitative index that measures these depths which is independent of reddening. This index is analogous to the Q index derived from UBV photometry which is used to determine spectral types for visible stars (e.g., Johnson & Morgan 1953). Using the average values of relative flux density calculated in three narrow bands, F1 ( $2.07\text{--}2.13\text{ }\mu\text{m}$ ), F2 ( $2.267\text{--}2.285\text{ }\mu\text{m}$ ), and F3 ( $2.42\text{--}2.46\text{ }\mu\text{m}$ ), we calculate the water vapor depth index  $W = (F1 - F3) / F2$ .

$\mu\text{m}$ ), and F3 (2.40–2.50  $\mu\text{m}$ ), we have defined a reddening-independent water index as

$$Q = (F1/F2)(F3/F2)^{1.22} \quad (1)$$

assuming a reddening law from 1.6–3.5  $\mu\text{m}$  of  $A_\lambda = \lambda^{-1.47}$  (Rieke & Lebofsky 1985, Cohen *et al.* 1981). A plot of the  $\text{H}_2\text{O}$  index  $Q$  vs. spectral type is shown in Fig. 3 for the M dwarf standards shown in Fig. 2. The error bars in the  $Q$  values are calculated from the statistical errors in the average flux values of F1, F2, and F3. The plot shows that  $Q$  appears to be linear from spectral type M0 to M8 but may start to flatten by M9. A weighted linear least squares fit to the M standard star data (excluding the K5V star Gl 775 and  $>\text{M9.5V}$  star BRI 0021-0214) data yields the following relation:

$$MV \text{ subclass} = (-18.35 \pm 1.72) \times Q + (17.00 \pm 0.45) \quad (2)$$

with a correlation coefficient of  $r=0.98$ . We expect that this relation cannot be used for spectral classification of objects with very strong CO bands, such as those found in late-type giants, as the higher vibrational first overtone bands become evident in the 2.4–2.5  $\mu\text{m}$  region. The application of this relation to spectral classifications of the brown dwarf candidate spectra is discussed in the following section.

### 3.2. Spectral Classifications of Brown Dwarf Candidates

Photospheric absorption lines characteristic of cool, late-type stars were observed in 15 of the 20 spectra of  $\rho$  Oph objects. However, placing these objects on the H–R diagram requires a two-step process; i) deriving spectral types for individual objects from comparison with spectral standards; and ii) adopting a temperature scale appropriate for the sample in question. The spectral classification of these objects is described below in Sec. 3.2.1. The effects on the derived spectral types of spectral veiling by circumstellar dust and of surface gravities less than those of dwarf stars are discussed in Sec. 3.2.2 and Sec. 3.2.3, respectively. We defer discussion of the effects of surface gravity on our adopted temperature scale to Sec. 4. Of the remaining 5 objects lacking evidence for late-type photospheres, GY 30 displayed a featureless spectrum and WL 18 has  $\text{Br}\gamma$  emission in an otherwise featureless spectrum (see also Greene & Lada 1996). The S/N in the spectrum for GY 218 ( $K=14.4$ ) was insufficient to attempt any classification. Finally upon further analysis, two objects (CRBR 1 and 2316.6-2131) showed  $\text{Br}\gamma$  absorption characteristic of stars of spectral type earlier than G0. These objects are discussed in Sec. 3.3.3.

### 3.2.1. Analysis of Water Vapor Features

Fifteen of the  $\rho$  Oph objects have spectra displaying absorption by CO, Na I, Ca I, and H<sub>2</sub>O as expected from late-type photospheres. Their composite CO equivalent widths (sum of  $\nu=0\text{--}2$  and  $2\text{--}4$ ) range from  $>6.5$  Å (GY 59) to  $>25$  Å (GY 107) with a median value of 12.5 Å. With the possible exception of GY 107, these equivalent widths are consistent with those observed in M dwarf stars. However, they are inconsistent with CO equivalent widths expected in M giants with strong water vapor absorption bands (e.g., Fig. 7 of Greene & Lada 1996). CO band absorption in the 2.4–2.5  $\mu\text{m}$  region is present in GY 107, and may cause the Q index and the photospheric temperature to be underestimated. For most sources in our sample, which appear to be late-type dwarfs, the CO absorption from 2.4–2.5  $\mu\text{m}$  has a negligible effect on the water-vapor index. Thus we conclude that most of the 15 objects in our sample are candidate very low mass stars and that our dwarf star calibration of the Q index introduced above is appropriate for estimating their spectral types.

We assume that the observed absorption features arise from some combination of a YSO photosphere plus possible contribution from continuum dust emission and not from a disk photosphere. While optically-thick continuum dust emission is commonly observed toward actively accreting T Tauri stars (Strom *et al.* 1989; Beckwith *et al.* 1990), optically-thick gas emission is thought to dominate near-IR emission only for objects with very high disk accretion rates such as the FU Ori class of eruptive variables (Kenyon & Hartmann 1996). Comparison of the CO equivalent widths for our candidate brown dwarfs with the sample of FU Ori stars studied by Greene & Lada (1996) at low resolution suggests that none of our objects belong to this rare class of objects. However, water vapor absorption can also arise in circumstellar disks surrounding less extreme PMS stars under certain conditions according to the models of Calvet *et al.* (1992). Features due to water vapor can contribute as much as 10% of the observed flux for accretion rates  $10^{-8}$   $M_\odot \text{ yr}^{-1}$  only if the circumstellar disk extends all the way into the stellar surface. At an accretion rate of  $10^{-7} M_\odot \text{ yr}^{-1}$ , water vapor becomes significant only for disks that extend to within  $2 R_*$ . Note that these calculations assume a central stellar temperature of 4000 K. A cooler central star will have a colder disk, making it less likely that inner disk will reach temperatures where gas opacity is dominant ( $> 1000$  K). Whether it is because disk accretion rates are typically  $< 10^{-7} M_\odot \text{ yr}^{-1}$  (Hartmann *et al.* 1998), or inner disks have inner holes  $> 2R_*$  (Meyer *et al.* 1997), it appears that the near-IR spectra of most YSOs are dominated by star+continuum dust emission rather than disk photospheres (Casali & Eiroa 1996; Greene & Lada 1997).

We have computed the reddening-independent water vapor index Q for each object in our sample using Eqn. 1. Using the relation between the water vapor index and MV

subclass (Eqn. 2), spectral types were computed for each brown dwarf candidate. We considered whether or not our water vapor index could have been influenced by our telluric correction procedure. An analysis of the derived Q values as a function of airmass difference between program object and telluric standard shows no correlation. Considering the uncertainties in the Q values and in the coefficients of eqn. 2, the spectral types are thought to be accurate to  $\pm 1.5$  subclasses. Q values and spectral types are presented in Table 2. The derived spectral types vary from M2.5 to M8.5. Ten of the objects have spectral types of M6 or later. Spectra of these objects are presented in Figures 4a and 4b. For comparison, we display spectra of M dwarf standards, artificially reddened using a  $\lambda^{-1.47}$  law, that provide a good match to the shape of the continuae of the brown dwarf candidates.

The optical spectrum of GY 5, shown in Fig. 5, gives us an opportunity to check the viability of the spectral types determined for the reddened brown dwarf candidates using the water vapor index. We compared our optical spectrum of GY 5 with dwarf and giant star standards of Kirkpatrick *et al.* (1991). Based on the relative strength of surface gravity sensitive features (e.g., Na I at  $\lambda 8183 \text{ \AA}$ ), GY 5 appears to be intermediate between luminosity class III and V as expected for a PMS star sitting above the main sequence. Similar behavior is reported by Luhman *et al.* (1997) for another brown dwarf candidate identified in the Ophiuchus dark cloud and observed with the same instrument. However, based upon the behavior of molecular features such as TiO and VO, GY 5 appears to be closer to the dwarf sequence. As shown in Fig. 5, a comparison of our spectrum with the dwarf standards of Kirkpatrick *et al.* (1991) suggests a spectral type of  $M6 \pm 1.0$  for GY 5. This agrees well with the spectral type derived above using the Q index ( $M7 \pm 1.5$ ). We note the absence H $\alpha$  in emission with the  $\text{EW}(\text{H}\alpha) < 5 \text{ \AA}$ .

### 3.2.2. Effects of Veiling

Although the computed H<sub>2</sub>O index Q is insensitive to reddening by interstellar extinction, other effects may cause variations in Q between stellar standards and PMS stars of identical spectral type. One major concern alluded to above is wavelength-dependent infrared excess due to thermal emission from warm dust grains in the circumstellar environments of the PMS stars. A geometrically-thin, optically-thick circumstellar disk is expected to exhibit an IR spectral shape characterized by  $F_\lambda \propto \lambda^{-7/3}$ , whether heated via viscous accretion or passive reprocessing (Lynden-Bell & Pringle 1974; Adams, Lada, & Shu 1987). We adopted this function to simulate the spectrum of a circumstellar disk at each observed wavelength in our spectral bandpass. We divided the resulting spectrum by a T=9000 K Planck function in order to process it comparably to the observed spectra

which have been divided by the spectrum of a dwarf star (usually near A0V) for telluric correction.

What is the magnitude of the effect of thermal emission by dust on spectral types derived using the water vapor index  $Q$ ? K band excess emission can be characterized by  $r_k = F_{Kex}/F_{K*}$ , where  $F_{Kex}$  is the broadband flux from excess (circumstellar) emission and  $F_{K*}$  is stellar flux at 2.2  $\mu\text{m}$ . Meyer *et al.* (1997) found that classical T Tauri stars have a median value of  $r_k \simeq 0.6$ , while weak-emission T Tauri stars have a median value of  $r_k \simeq 0.0$ . In order to simulate this range of excesses, we scaled a normalized disk spectrum to equal 0.2 and 0.6 times the flux of several standard star spectra at  $\lambda = 2.20\mu\text{m}$ . These scaled model disk spectra were then added to those of the standard stars, resulting in spectra which are representative of PMS stars whose K band emissions arise from both stellar photospheres and disks. We then recomputed the  $Q$  indices of these resultant spectra and found that  $Q$  increased (implying earlier spectral types) over that of the same standards without this excess emission added. Both the M6.5V (GJ 1111) and M9V (LHS 2924) standards appeared to have  $Q$ -derived spectral types 1 subclass earlier when  $r_k = 0.2$  disk spectra were added, and spectral types 3 subclasses earlier when  $r_k = 0.6$  disk spectra were added.

We have estimated the minimum likely K band excess,  $r_k$ , for each brown dwarf candidate from published near-infrared photometry and include these results in Table 2. These estimates are minima because our calculations assume that the candidates have no excesses in the  $J$  or  $H$  bands. The K excess is estimated from  $r_k = 10^{0.4 \times E(H-K)_0} - 1$ , where  $E(H - K)_0 = (H - K) - 0.065A_v - (H - K)_0$  (e.g., Meyer *et al.* ). The value of  $r_k$  is less than 0.3 for all sources except for CRBR 15, GY 11, GY 64, and GY 202, which have values similar to those of classical T Tauri stars. Thus the  $Q$ -derived spectral types of most brown dwarf candidates in the sample should be unaffected by emission from circumstellar dust, but CRBR 15, GY 11, GY 64, and GY 202 may have actual spectral types which are 2–3 subclasses later than those presented in Table 2.

### 3.2.3. Surface Gravity Effects

We have compared the spectra of our brown dwarf candidates to a sequence of dwarf standards rather than giants. Yet surface gravities for PMS stars are known to be intermediate between those of dwarfs and giants (e.g., Schiavon, Batalha, & Barbuy 1995). Spectroscopic studies indicate that the surface gravities of PMS stars are most similar to those of main sequence dwarfs (Basri & Batalha 1990; Greene & Lada 1997). This is consistent with our analysis of the composite CO equivalent widths in our sample and the

GY 5 spectrum. If the brown dwarf candidates have surface gravities of subgiants, how would this effect our derived spectral types? Absorption in the  $1.9 \mu\text{m}$  water vapor band is generally weaker in late-type giants than in dwarf stars of the same spectral type (e.g., Aaronson, Frogel, & Persson 1978, Kleinmann & Hall 1986). Only for the latest spectral types ( $>\text{M}6$ ) is the water band similar in depth for dwarfs and giants. Hence, we may have systematically classified stars 1–2 subclasses earlier than appropriate for stars  $<\text{M}6$  by assuming dwarf rather than subgiant surface gravities. Classifications of stars M6 or later appear to be nearly independent of surface gravity. Higher resolution data, obtainable with the next generation of 8–10 m class telescopes, are required in order to perform a detailed analysis of the surface gravities of very low mass PMS objects. Note that there is still an open question of surface gravity effects on our translation of spectral types to effective temperatures. We defer this discussion to Sec. 4.

### 3.3. Notes on Individual Sources

#### 3.3.1. GY 11

The infrared spectrum of GY 11 (Fig. 4b) shows absorption bands of CO and  $\text{H}_2\text{O}$ , modified by the presence of dust emission. Its infrared excess is confirmed through weak  $\lambda=10 \mu\text{m}$  emission (Rieke & Rieke 1990) and recent ISOCAM observations (Comerón *et al.* 1998). In addition, emission lines due to  $\text{H}_2$  are also present: the  $1 \rightarrow 0$  S(1) at  $2.122 \mu\text{m}$  and the  $1 \rightarrow 0$  Q-branch lines at  $2.407$ ,  $2.413$ , and  $2.424 \mu\text{m}$ . Emission from the  $1 \rightarrow 0$  S(1) transition has been previously reported by Williams *et al.* (1995). Such emission line spectra are characteristic of YSOs with molecular outflows (Reipurth & Aspin 1997; Greene & Lada 1996) and could be evidence that the low-luminosity PMS star GY 11 has an associated outflow. A second possibility is that the  $\text{H}_2$  emission is due to a chance coincidence between GY 11 and an  $\text{H}_2$  emission knot from the VLA 1623 outflow. As seen in deep  $\text{H}_2$  images, there is a “stream” of  $\text{H}_2$  emission between VLA 1623 and  $\text{H}_2$  knot H4 that intersects the position of GY 11 (see Fig. 7 of Dent, Matthews, & Walters 1995).

#### 3.3.2. Possible Background Stars CRBR 1 & 2316.6-2131

While not shown here, both CRBR 1 and 2316.6-2131 display spectra with  $\text{Br } \gamma$  absorption and no CO bands. This suggests they have spectral types of G0 or earlier (e.g., Ali *et al.* 1995; Wallace & Hinkle 1997). Adopting intrinsic colors appropriate for this inferred range of spectral types, neither object exhibits an infrared excess at K; their color

excess ratios,  $E(J - H)/E(H - K)$ , are consistent with the value of  $1.57 \pm 0.03$  derived for the Ophiuchus cloud by Kenyon, Lada, & Barsony (1998). From their observed  $(H - K)$  color, the visual extinctions toward CRBR 1 and 2316.6-2131 are estimated to be  $A_v \sim 22^m$  and  $\sim 25^m$ , respectively. The observed slopes of the continuae in their infrared spectra are consistent with the spectrum of an early-type star reddened by these amounts. Given the early spectral types and lack of infrared excess, it is possible that CRBR 1 and 2316.6-2131 are background stars viewed through the dark cloud. Indeed, the visual extinctions we estimate are consistent with the total cloud extinction of  $A_v = 36 \pm 18^m$  estimated from the  $\text{C}^{18}\text{O}$  column densities along the lines of sight to each source (Wilking & Lada 1983).

### 3.3.3. Possible Background Giant GY 107

The infrared spectrum of GY 107 shows the signatures of a late-type photosphere including strong CO band absorptions. Near-infrared photometry indicates it does not have an infrared excess. The visual extinction estimated to this source of  $A_v = 13^m$  is consistent with the total cloud extinction of  $15 \pm 8^m$  estimated from the  $\text{C}^{18}\text{O}$  column density along this line of sight. Therefore it is possible that GY 107 is a background star viewed through the dark cloud. The strengths of the CO bands are consistent with a K5-M0III classification and not the M3V classification derived from the Q index (e.g., Fig. 4 in Greene & Lada 1996). A giant classification would imply a distance greater than 1 kpc, consistent with being a background star.

## 4. Masses and Ages of the Brown Dwarf Candidates

To place the brown dwarf candidates on a Hertzsprung-Russell (H-R) diagram and estimate their masses and ages requires us first to convert their spectral types to effective temperatures and to determine their bolometric luminosities. The adopted temperature scale for M dwarfs is based on the modified blackbody fits of Jones *et al.* (1996) and is derived in Appendix A. Effective temperatures computed for each brown dwarf candidate are given in Table 2 and have typical uncertainties in the Log of  $\pm 0.035$  dex, dominated by the uncertainty in computing each value of Q. However, systematic effects could affect the derived effective temperatures. As alluded to in Sec. 3.2.2, effective temperatures for CRBR 15, GY 11, GY 64, and GY 202 could be overestimated by 300-500K due to the presence of veiling. The assumption of dwarf, rather than subgiant, surface gravities could also systematically effect our results. Because late-type giant star temperatures are 300-500 K higher than the adopted dwarf temperature scale (compare Table 5 with the

giant temperature scale in Perrin *et al.* 1998), we may be underestimating the effective temperature by  $\sim$ 150–250 K for stars later than M6. For stars classified as M2–M6, the temperatures quoted here should not be systematically off since the higher effective temperature scale for subgiants is compensated for by the later spectral type needed to produce the same water vapor absorption (Sec. 3.2.3). With these caveats in mind, we adopt the temperatures listed in Table 2 for our brown dwarf candidates.

Given their spectral types, bolometric luminosities were estimated for each brown dwarf candidate by i) dereddening their J magnitudes using the corresponding intrinsic ( $J - H$ ) colors for M dwarfs; ii) applying bolometric corrections to the J magnitudes appropriate for each spectral type; and iii) converting absolute magnitudes to bolometric luminosities using the standard relation  $\text{Log}(L_{bol}/L_{\odot}) = 1.89 - 0.4 \times M_{bol}(\ast)$ . Infrared photometry for the brown dwarf candidates is presented in Table 2 and is from the study of Barsony *et al.* (1997) in the CIT photometric system. Intrinsic colors and bolometric corrections as a function of MV subclass were derived using the studies of Leggett (1992), Tinney, Mould, & Reid (1993) and Leggett *et al.* (1996); the derivation of these values is described in Appendix A. For two sources without J photometry, bolometric luminosities were estimated in the same manner from the H and K photometry. Visual extinctions could be overestimated for objects with excess emission at H resulting in overestimates for  $\text{Log}(L_{bol}/L_{\odot})$  by about 0.25 dex (0.1 dex) assuming  $r_h=0.6$  ( $r_h=0.2$ ). Values for  $\text{Log}(L_{bol}/L_{\odot})$  are presented in Table 2 and have formal uncertainties of  $\pm 0.16$  dex.

H–R diagrams for the 15 brown dwarf candidates are shown in Figure 6 for two sets of theoretical tracks. Fig 6a. shows their placement relative to the evolutionary tracks and isochrones of D’Antona & Mazzitelli (1998) from 0.02 and 0.3  $M_{\odot}$ . The models use opacities from Alexander & Ferguson (1994) and the Full Spectrum of Turbulence convection model of Canuto & Mazzitelli (1991) and assume mass fractions of helium, metals, and deuterium of  $Y=0.28$ ,  $Z=0.02$ , and  $X_D=2 \times 10^{-5}$ . These models are similar to those described in D’Antona & Mazzitelli (1997), but with an improved treatment of deuterium burning. Fig. 6b shows the candidates on a H–R diagram alongside the theoretical tracks of Burrows *et al.* (1997) for masses between 0.01 and 0.24  $M_{\odot}$ . These models are constructed specifically for substellar objects and consider a variety of opacity sources, particularly water vapor, and assume mass fractions of helium, metals, and deuterium of  $Y=0.25$ ,  $Z=0.02$ , and  $X_D=2 \times 10^{-5}$ .

The masses and ages derived for our brown dwarf candidates from both models are presented in Table 3. Regardless of choice of tracks, one sees that the majority of objects do appear to have ages of  $10^6$  years or less, with a median age of  $3\text{--}4 \times 10^5$  years. These ages agree with those derived for more massive cluster members by Greene & Meyer based on the

D'Antona & Mazzitelli (1994) tracks<sup>5</sup>. This agreement gives one confidence in the adopted models but one must bear in mind that while the relative ages may be robust, absolute ages are model dependent and difficult to verify by independent means (see for example Fig. 5 in Luhman & Rieke 1998). The apparent older age for GY 11 is most likely a result of its veiled photosphere which leads us to overestimate its effective temperature. *Six of the brown dwarf candidates, CRBR 14, GY 10, GY 11, GY 64, GY 202, and GY 310, consistently fall below the hydrogen burning limit of  $0.08 M_{\odot}$ , taking into account the uncertainties in their effective temperatures.* To be consistent in age with the other candidates, GY 11 must have a mass in the range  $<0.02 M_{\odot}$ . In addition, the brown dwarf candidates CRBR 15, GY 5, GY 37, GY 59, and GY 84 lie in the transition region between stellar and substellar objects and we cannot rule out that some are brown dwarfs. Again, masses derived from PMS models require independent confirmation by studies of PMS binary stars (Ghez *et al.* 1995) or other techniques (Bonnell *et al.* 1998). The range of masses derived from both sets of tracks considered here gives some indication of the uncertainties in the mass estimates (see Table 3).

## 5. Discussion

In the previous section, we demonstrated that six of our candidate objects appear to be brown dwarfs according to the PMS tracks considered. An additional five stars in our sample lie at the stellar–substellar boundary at an age of  $< 10^6$  yrs. What can we say about the nature of these very low mass objects? By studying these and other recently discovered young brown dwarfs in more detail, we hope to learn whether very low mass stars are assembled in a similar fashion to higher mass stars. We conclude with a discussion of how purely photometric techniques compare with our mass estimates based on spectroscopy.

### 5.1. Infrared Excesses for Substellar Objects

Do young brown dwarfs exhibit infrared excess emission characteristic of active accretion disks? If PMS stars of masses  $0.5–1.0 M_{\odot}$  evolve from  $0.1 M_{\odot}$  protostars with massive accretion disks, perhaps the lowest mass association members are those that form without significant disk accretion. In our sample, CRBR 15, GY 11, GY 64, and GY 202 have obvious  $2.2 \mu\text{m}$  excesses (lower limits are given in Table 2 as  $r_k$ ). This group includes

---

<sup>5</sup>The D'Antona & Mazzitelli (1998) tracks used in our analysis are identical to their 1994 models for  $M > 0.2 M_{\odot}$ .

three of our six probable brown dwarfs. These  $2.2 \mu\text{m}$  excesses are confirmed by combining near-infrared data and our effective temperature estimates with ISOCAM observations in the thermal IR (Comerón *et al.* 1998). In addition, an excess is suggested for CRBR 14 at wavelengths beyond  $5 \mu\text{m}$ , indicating the presence of an inner hole in the circumstellar dust distribution. Finally we note that the  $\rho$  Oph brown dwarf studied by Luhman *et al.* (1997) exhibits strong  $\text{H}\alpha$  emission as well as thermal IR excess emission, suggesting the presence of an accretion disk. In summary, indications are that brown dwarfs in the Ophiuchus dark cloud can indeed possess active accretion disks analogous to those found around higher mass PMS stars.

Using excess emission at  $\lambda=2.2 \mu\text{m}$  to identify circumstellar disks among members of the ONC, Hillenbrand *et al.* (1998) find a lower disk frequency for the lowest mass cluster members ( $M < 0.2 M_\odot$ ); a disk frequency of only 20–50% is estimated for substellar objects compared to 55–90% for the cluster as a whole. Hillenbrand *et al.* forward several possible explanations for this lower frequency including smaller disk masses, lower disk accretion rates, and/or a higher incidence of disk stripping for the lowest mass cluster members. By identifying a statistically significant sample of brown dwarfs in the core of the Rho Oph cloud, this latter hypothesis can be tested in a cluster of approximately the same age as the ONC. Stellar encounters and the stripping of circumstellar disks would be less prevalent in the lower stellar density environment of the Rho Oph core whose stellar density is a factor of  $\sim 50$  times lower than the ONC density of  $\sim 5 \times 10^4 \text{ pc}^{-3}$ .

## 5.2. Comparisons of Spectroscopic and Photometric Techniques

Even though spectroscopy affords the most reliable way to estimate effective temperatures of stars and young brown dwarfs, it has limitations. First, while optical spectroscopy provides the best studied sets of lines for spectral classification, the visual extinction in a star-forming cloud severely limits the number of young brown dwarfs that can be observed at  $R \sim 1000$  in the R and I bands. Among the 15 brown dwarf candidates in this study, only six (with extinctions less than  $13^m$ ) appear in an I band image of the cloud ( $I < 19^m$ , Wilking *et al.* 1998) and are accessible targets for moderate resolution spectroscopy on a 4-m class telescope. Second, even infrared spectroscopy is currently limited to low-luminosity objects near the surface of the cloud. In our study, the probable brown dwarfs range in extinction from  $5$ – $14^m$  while the total extinction in the core is estimated to be  $50$ – $100^m$ . Brown dwarfs throughout most of the cloud volume are below the detection limit even for low resolution infrared spectroscopy with a 3–4 m class telescope.

Ultimately, any study of the mass functions of young clusters down to substellar

masses will have to combine sensitive photometric surveys with spectroscopic data. The main disadvantage of analyzing photometric data alone is that mass and age cannot be uniquely determined. Typically one either assumes an input mass distribution and derives an age from fits to PMS evolutionary tracks (e.g., Lada & Lada 1995) or one assumes an age distribution and derives the mass function (e.g., Comerón, Rieke, & Rieke 1996). The addition of spectroscopic information permits one to construct an H–R diagram for some fraction of the photometric sample in order to estimate the age distribution of the cluster, crucial for adopting the appropriate mass–luminosity relationship (e.g., Meyer 1996). Given this age distribution, the derived distribution of stellar masses should reflect the cluster mass function for a large statistical sample.

How do determinations of mass made with infrared spectra compare with those determined from infrared photometric data? For example, the color-magnitude diagram in Fig. 1 based upon the D’Antona & Mazzitelli models would predict that for an age of  $3 \times 10^5$  years, 15 of the 20 brown dwarf candidates (75%) have masses  $\leq 0.1 M_{\odot}$ . Using the infrared spectra and the same input models, we have determined that 11 of 14 (79%) candidates have  $M \leq 0.1 M_{\odot}$ , with three of the brown dwarf candidates identified as possible background stars. One of the important advantages of infrared spectroscopy is the ability to reduce contamination of the sample by field stars.

A recent photometric study by Comerón *et al.* (1998) used model fits of the SEDs of Ophiuchus brown dwarf candidates, extended to mid-infrared wavelengths by ISOCAM data at  $\lambda = 3.6 \mu\text{m}$ ,  $4.5 \mu\text{m}$ , and  $6.0 \mu\text{m}$ , to estimate effective temperatures. They utilized the Burrows *et al.* (1997) models to estimate mass assuming an age of either  $10^6$  or  $3 \times 10^6$  years. The distribution of sources in our H–R diagram (Fig. 6) suggests that ages ranging from  $10^5$  to  $10^6$  years would be more appropriate and would tend to give lower mass estimates than those quoted by Comerón *et al.* Seven objects are in common between this study and Comerón *et al.*, including five of the six probable brown dwarfs identified in our study. In general, the temperatures derived by their SED models are systematically higher by several hundred K compared to those suggested from the infrared spectra, but usually within the stated uncertainty of our technique. Notable exceptions include GY 10 and CRBR 14; the photometric technique derives an effective temperature for GY 10 which is 700 K hotter than indicated from the near-infrared spectrum and 350 K hotter for CRBR 14. Masses derived by the Comerón *et al.* study are typically a factor of two greater than we derive from the same PMS tracks (Burrows *et al.* models; see col. 4–5, Table 3) with larger differences evident for CRBR 14, CRBR 15, and GY 10. In the case of CRBR 15, the higher mass derived by Comerón *et al.* ( $0.23 M_{\odot}$  vs.  $< 0.09 M_{\odot}$  from this study) arises from using a higher visual extinction than we estimate from the (J–H) color and spectral type. Their model appears to overestimate the luminosity of the star

while underestimating the contribution to the bolometric luminosity from infrared excess emission. In summary, our mass estimates usually agree within a factor of two of those derived by SED fitting, although they are systematically lower as expected given that the objects appear to be cooler and slightly younger than assumed by Comerón *et al.*

## 6. Summary

We have obtained low resolution infrared spectra for 20 brown dwarf candidates which lie toward the core of the  $\rho$  Ophiuchi dark cloud and for 14 late-type spectral standards. Analysis of these spectra, in combination with published near-infrared photometry, has enabled us to derive effective temperatures and bolometric luminosities for the brown dwarf candidates. Utilizing the PMS evolutionary models of Burrows *et al.* (1997) and D'Antona & Mazzitelli (1998), we estimate masses and ages for the sample, as well as consider the distribution of circumstellar material around these low mass young stars. Our analysis has yielded the following results:

- We have developed a novel technique that uses the infrared water vapor bands to derive spectral types for M dwarfs, independent of reddening, to within  $\pm 1.5$  subclasses. An optical spectrum obtained for one brown dwarf candidate, GY 5, confirms the spectral classification derived from the water bands.
- Fifteen of the brown dwarf candidates display photospheric absorption features characteristic of late-type stars and all but one appear to be low mass members of the  $\rho$  Ophiuchi cloud. The derived spectral types range from M2.5–M8.5. The presence of veiling in four of the objects leads us to derive spectral types which are too early by 2–3 subclasses. The brown dwarf candidate GY 107 is identified as a possible background giant.
- An H–R diagram of the brown dwarf candidates indicate that six are substellar in nature for both of the evolutionary models considered here. Another five candidates lie in the transition region between stellar and substellar objects. The median age for the sample is  $3\text{--}4 \times 10^5$  years, consistent with the ages determined for more massive PMS objects in the cloud.
- Three of the probable brown dwarfs display infrared excesses at  $\lambda=2.2\text{ }\mu\text{m}$  and four have excesses at mid-infrared wavelengths. By analogy with classical T Tauri stars in the Taurus dark cloud, the near-infrared colors of these objects suggest that young brown dwarfs in this cloud can have active accretion disks.

Future studies of the emergent mass distribution in  $\rho$  Oph will require combining

spectroscopic studies such as this, with deep infrared imaging photometry in order to constrain the mass function below the hydrogen burning limit. Follow-up observations aimed at characterizing the distribution of circumstellar material surrounding these very young brown dwarfs will be extremely useful in constraining models of very low mass star formation.

We would like to thank Jim Liebert, Kevin Luhman, and George Rieke for important discussions that guided the interpretation of these data. We especially thank John Carpenter who assisted in formulating the candidate list and Joan Najita who suggested using water vapor bands for spectral classification. We are grateful to Kevin Luhman and Lynne Hillenbrand for providing electronic versions of the Kirkpatrick et al. standards and assistance with the spectral classification of GY 5. David Sing and Ale Milone provided expert assistance in obtaining the spectrum of GY 5 during the last hour of the last night of the last regularly scheduled run of the old MMT. Mary Barsony generously provided infrared photometry in advance of publication. We thank the IRTF and telescope operators Bill Golisch and Charlie Kaminski for performing service observations for two standard stars. B.W. gratefully acknowledges the support of RUI Grant NSF AST-9417210 to the University of Missouri-St. Louis. Support for MRM was provided by NASA through Hubble Fellowship grant # HF-01098.01-97A awarded by the Space Telescope Institute, which is operated by the Association of Universities for Research in Astronomy, Inc., for NASA under contract NAS 5-26555.

#### A. Adopted Temperature Scale, Intrinsic Colors, and Bolometric Corrections for M Dwarfs

In order to use infrared spectra and broadband near-infrared photometry to place our brown dwarf candidates in an H-R diagram, we need to adopt a temperature scale, intrinsic  $(J - H)_0$  and  $(H - K)_0$  colors, and bolometric corrections at J ( $1.25\mu\text{m}$ ) and K ( $2.2\mu\text{m}$ ) for each spectral type. No single modern compilation of these values exists for M dwarfs, so we developed our own based on recent data presented in the literature. For consistency, we have used the M dwarf spectral classifications of Kirkpatrick, Henry, & McCarthy (1991) and Henry, Kirkpatrick, & Simons (1994). To minimize the effects of metallicity, only stars classified as disk objects based on kinematics were considered (Leggett 1992). Our temperature scale for M dwarfs was established using the modified blackbody fits in Table 3 of Jones *et al.* (1996). Their stated random error in the determination of temperature scales is  $\Delta T_{eff} = 150$  K. We chose their temperatures over those derived by other studies as they included three dwarfs of very late spectral type (M8, M8.5 and M9) and did not rely

on fitting of synthetic spectra which currently have trouble reproducing spectral features in very late M dwarfs. Intrinsic  $(J - H)$  and  $(H - K)$  colors were taken from Leggett (1992) and Leggett *et al.* (1996) and are in the CIT photometric system. Bolometric corrections at K were taken from Leggett *et al.* (1996) and Tinney, Mould, & Ried (1993) and are also in the CIT system. Bolometric corrections at J were derived using the  $(J - K)$  colors and  $M_K$ . Table 4 summarizes the temperatures, intrinsic colors, and bolometric corrections compiled for individual stars.

To derive a temperature scale, and continuous intrinsic  $(J - H)$  and  $(H - K)$  colors and bolometric corrections as a function of M spectral class, uniform-weighted fits were made to the data in Table 4 over the spectral range M2V–M9V. A linear least squares fit to the Jones *et al.* temperatures yields the following temperature scale:

$$T_{eff} = (-166 \pm 8) \times (MV \text{ subclass}) + (3758 \pm 52)K. \quad (\text{A1})$$

A linear fit to the  $(J - H)$  and  $(H - K)$  color vs. MV subclass yields the following relations:

$$(J - H)_0 = (0.0187 \pm 0.0047) \times (MV \text{ subclass}) + (0.503 \pm 0.026) \quad (\text{A2})$$

$$(H - K)_0 = (0.0437 \pm 0.0023) \times (MV \text{ subclass}) + (0.096 \pm 0.012). \quad (\text{A3})$$

A linear fit to the K bolometric corrections,  $BC_K$ , results in the following relation:

$$BC_K = (0.0895 \pm 0.0065) \times (MV \text{ subclass}) + (2.43 \pm 0.04). \quad (\text{A4})$$

A second order fit was needed for the J bolometric corrections,  $BC_J$ , as the peak flux of the M2–M9 dwarfs moves completely through the J band. The fit yielded:

$$BC_J = (-0.0105 \pm 0.0034) \times (MV \text{ subclass})^2 + (0.148 \pm 0.040) \times (MV \text{ subclass}) + (1.53 \pm 0.10). \quad (\text{A5})$$

While the  $(J - H)_0$  dependence with spectral type appears double-valued over a broader range of spectral types (e.g., Bessell & Brett 1988), it is best represented by a linear fit over our range of MV subclasses. of wavelength, it is best fit by The adopted values for effective temperature,  $(J - H)_0$ ,  $(H - K)_0$ ,  $BC_J$ , and  $BC_K$  are given in Table 5 from M2V to M9V in increments of 0.5 subclasses.

## REFERENCES

Adams, F. , Lada, C., & Shu, F. 1987, ApJ, 213, 788  
 Alexander, D. R. & Ferguson, J. W. 1994, ApJ, 437, 879

Ali, B., Carr, J., DePoy, D., Frogel, J., & Sellgren, K. 1995, AJ, 110, 2415

Aaronson, M., Frogel, J. A., & Persson, S. E. 1978, ApJ, 220, 442

Barsony, M., Burton, M., Russell, A. P. G., & Garden, R. 1989, ApJ, 346, L93

Barsony, M., Kenyon, S., Lada, E., & Teuben, P. 1997, ApJS, 112, 109.

Basri, G. & Batalha, C. 1990, ApJ, 363, 654

Beckwith, S. V. W., Sargent, A. I., Chini, R., & Güsten, R. 1990, AJ, 99, 924

Bessell, M. S. & Brett, J. M 1988, PASP, 100, 1134

Bonnell, I. A., Smith, K. W., Meyer, M. R., Tout, C. A., Folha, D. F. M., & Emerson, J. P. 1998, MNRAS, in press

Briceño, C., Hartmann, L., Stauffer, J., & Martín, E., 1998, AJ, in press

Burrows, A., Marley, M., Hubbard, W. B., Lunine, J. L., Guillot, T., Saumon, D., Freedman, R., Sudarsky, D., & Sharp, C. 1997, ApJ, 491, 856

Calvet, N., Magris, G., Patino, A., & D'Alessio, P. 1992, RMXA&A, 24, 27

Canuto, V. M. & Mazzitelli, I. 1991, ApJ, 370, 295

Casoli, M. & Eiroa, C. 1996, A&A, 306, 427

Casanova, S., Montmerle, T., Feigelson, E. D., & André, P. 1995, ApJ, 439, 752

Cohen, J. G., Frogel, J. A., Persson, S. E., & Elias, J. H. 1981, ApJ, 249, 481

Comerón, F., Rieke, G. H., Burrows, A., Rieke, M. J. 1993, ApJ, 416, 185

Comerón, F., Rieke, G. H., & Rieke, M. J. 1996, ApJ, 473, 294

Comerón, F., Rieke, G. H., Claes, P., Torra, J., & Laureijs, R. J. 1998, A&A, in press

D'Antona, F. & Mazzitelli, I. 1994, ApJS, 90, 467

D'Antona, F. & Mazzitelli, I. 1997, in Cool Stars in Clusters and Associations, eds. R. Pallavicini & G. Micela, Mem. S. A. It., 68, n.4.

D'Antona, F. & Mazzitelli, I. 1998, priv. comm.

Dent, W. R. F., Matthews, H. E., & Walther, D. M. 1995, MNRAS, 277, 193

de Zeeuw, P. T., Brown, A. G. A., de Bruijne, J. H. J., Hoogerwerf, R., Lub, J., Le Poole, R. S., & Blaauw, A. 1997, ESA SP-402, 495

Ghez, A. M., Weinberger, A. J., Neugebauer, G., Matthews, K., & McCarthy, D. W. 1995, AJ, 110, 753

Grasdalen, G. L. Strom, K. M., & Strom, S. E. 1973, ApJ, 184, L53

Greene, T. P. & Lada, C. J. 1996, AJ, 112, 2184

Greene, T. P. & Lada, C. J. 1997, AJ, 114, 2157

Greene, T. P. & Meyer, M. R. 1995, ApJ, 450, 233

Greene, T. P. & Young, E. T., 1992, ApJ, 395, 516

Hartmann, L., Calvet, N., Gullbring, E., & D'Alessio, P. 1998, ApJ, 493, 909

Henry, T. J., Kirkpatrick, J. D., & Simons, D. A. 1994, AJ, 108, 1437

Hillenbrand, L. A. 1997, AJ, 113, 1733

Hillenbrand, L. A., Strom, S. E., Calvet, N., Merrill, K. M., Gatley, I., Makidon, R. B., Meyer, M. R., & Skrutskie, M. F. 1998, AJ, in press

Johnson, H. L. & Morgan, W. W. 1953, ApJ, 117, 313

Jones, H. R. A., Longmore, A. J., Allard, F., & Hauschildt, P. H. 1996, MNRAS, 280, 77

Kenyon, S. J. & Hartmann, L. 1996, ARA&A, 34, 207

Kenyon, S., Lada, E., & Barsony, M. 1998, AJ, 115, 252

Kirkpatrick, J. D., Beichman, C. A., & Skrutskie, M. F. 1997, ApJ, 476, 311

Kirkpatrick, J. D., Henry, T. J., & McCarthy, D. W. 1991, ApJS, 77, 417

Kleinmann, S. G., & Hall, D. N. B. 1986, ApJS, 62, 501

Lada, E. A., & Lada, C. J. 1995, AJ, 109, 1682

Leggett, S. K. 1992, ApJS, 82, 351

Leggett, S. K., Allard, F., Berriman, G., Dahn, C. C., Hauschildt, P. H. 1996, ApJS, 104, 117

Luhman, K. L., Liebert, J., & Rieke, G. H. 1997, ApJ, 489, L165

Luhman, K. L. & Rieke, G. H. 1998, ApJ, 497, 354

Luhman, K. L., Rieke, G. H., Lada, C. J., and Lada, E. A. 1998, ApJ, in press

Lynden-Bell, D. & Pringle, J. E. 1974, MNRAS, 168, 603

Meyer, M. R. 1996, Ph.D. thesis, University of Massachusetts

Meyer, M. R., Calvet, N., & Hillenbrand, L. A. 1997, AJ, 114, 288

Motte, F., André, P., & Neri, R. 1998, A&A, in press

Perrin, G., Coudé du Foresto, V., Ridgway, S. T., Mariotti, J.-M., Traub, W. A., Carleton, N. P., & Lacasse, M. G. 1998, A&A, 331, 619

Rayner, J. 1998, Proc. SPIE, in press.

Reipurth, B. & Aspin, C. 1997, AJ, 114, 2700

Rieke, G. H. & Lebofsky, M. J. 1985, ApJ, 288, 618

Rieke, G. H. & Rieke, M. J. 1990, ApJ, 362, L21

Scalo, J. 1998, in The Stellar Initial Mass Function, Proceedings of the 38th Hertsmonceux Conference, ed. G. Gilmore, I. Parry, & S. Ryan, in press

Schiavon, R. P., Batalha, C., Barbuy, B. 1995, A&A, 301, 840

Shure, M. A., Toomey, D. W., Rayner, J. T., Onaka, P. M., & Denault, A. J. 1994, Proc. SPIE, 2198, 614.

Strom, K. M., Strom, S. E., Edwards, S., Cabrit, S., & Skrutskie, M. 1989, AJ, 97, 1451

Strom, K. M., Kepner, J., & Strom, S. E. 1995, ApJ, 438, 813

Tinney, C. G., Mould, J. R., & Ried, I. N. 1993, AJ, 105, 1045

Vrba, F. J., Strom, S. E., Strom, K. M., & Grasdalen, G. L. 1975, ApJ, 197, 77

Wallace, L. & Hinkle, K. 1997, ApJS, 111, 445

Wilking, B. A. & Lada, C. J. 1983, ApJ, 274, 698

Wilking, B., Schwartz, R. D., Fanetti, T., & Friel, E. 1998, unpublished data.

Williams, D. M., Comerón, F., Rieke, G. H., and Rieke, M. J. 1995, ApJ, 454, 144

### Figure Captions

Fig. 1.— A color-magnitude diagram of the Ophiuchus brown dwarf candidates. All photometry is taken from the study of Barsony *et al.* (1997). Isochrones for stars of masses ranging from  $0.04\text{--}2.5 M_{\odot}$  were derived from the models of D'Antona & Mazzitelli (1994,  $M>0.2 M_{\odot}$ ) and D'Antona & Mazzitelli (1998,  $M\leq0.2 M_{\odot}$ ) in the CIT photometric system using intrinsic colors and bolometric corrections for dwarf stars derived in Appendix A. Isochrones are shown for  $3 \times 10^5$  years and  $5 \times 10^8$  years. Reddening lines from the  $3 \times 10^5$  year isochrone are shown for selected masses by dashed lines and were calculated using the extinction law derived by Cohen *et al.* (1981). For comparison, a reddening vector for an  $A_v=10^m$  is also shown.

Fig. 2.— Infrared spectra of M dwarf standards at  $R=300$ . Spectral types were adopted from Kirkpatrick, Henry, & McCarthy (1991) or Henry, Kirkpatrick, & Simons (1994). Fig. 2a shows the  $2.0\text{--}2.5 \mu\text{m}$  spectra for dwarfs from K5 to M4. Fig. 2b shows spectra for dwarfs of spectral type M4.5 to  $>M9.5$ . The wavelengths of absorption lines of Na, Ca, Mg, and CO are marked at the bottom of each plot. The wavelength ranges averaged to compute the water vapor index  $Q$  are labeled as F1, F2, and F3.

Fig. 3.— A plot of the water vapor index,  $Q$ , vs. MV subclass for our M dwarf standards. Spectral types were adopted from Kirkpatrick, Henry, & McCarthy (1991). Error bars reflect one-sigma uncertainties in  $Q$  from the statistical uncertainties in calculating F1, F2, and F3. The solid line is the best fit to the data (Eqn. 2).

Fig. 4.— Infrared spectra of selected brown dwarf candidates in the  $\rho$  Oph cloud at  $R=300$ . The water vapor index indicates these objects have spectral types  $\geq M6$ . Fig. 4a shows the  $2.0\text{--}2.5 \mu\text{m}$  spectra for candidates that most closely resemble the spectrum of the lightly reddened M7 dwarf shown at the bottom of the stack. The M dwarf spectrum was produced by artificially reddening our spectrum of Gl 644c by  $A_v=5^m$  assuming  $A_{\lambda} \propto \lambda^{-1.47}$ . Fig. 4b shows spectra for candidates most closely resembling the spectrum of the more heavily reddened M6 dwarf shown at the bottom of the stack. The M dwarf spectrum was produced by artificially reddening our spectrum of Gl 406 by  $A_v=10^m$ . The wavelengths of absorption lines of Na, Ca, Mg, and CO are marked at the bottom of each plot. The wavelength ranges averaged to compute the water vapor index  $Q$  are labeled as F1, F2, and F3.

Fig. 5.— An optical spectrum for the brown dwarf candidate GY 5 relative to dwarf spectral standards of Kirkpatrick *et al.* (1991). The spectrum of this PMS object appears intermediate to that of a M5.5 and M6 dwarf. Labeled on the plot are photospheric atomic absorptions due to K I, Na I, and Ca II and molecular absorptions from TiO and VO.

Features labeled as O<sub>2</sub> are telluric in nature. For a more complete identification of features, see Kirkpatrick *et al.* (1991), Fig. 5c.

Fig. 6.— Hertzsprung-Russell diagrams for the  $\rho$  Oph brown dwarf candidates. Fig. 6a shows the candidates relative to the theoretical tracks of D'Antona & Mazzitelli (1998). Fig. 6b shows the candidates relative to the theoretical tracks of Burrows *et al.* (1997). Isochrones from  $10^5$  years to  $10^8$  years are shown by solid lines and evolutionary tracks from  $0.02 M_{\odot}$  to  $0.30 M_{\odot}$  are shown by dashed lines. The bold dashed line marks the evolutionary track for a star at the hydrogen-burning limit. The typical error bar for a candidate is shown in the lower left of each plot and is  $\pm 0.035$  dex in  $\log(T_{eff})$  and  $\pm 0.16$  dex in  $\log(L_{bol}/L_{\odot})$ .

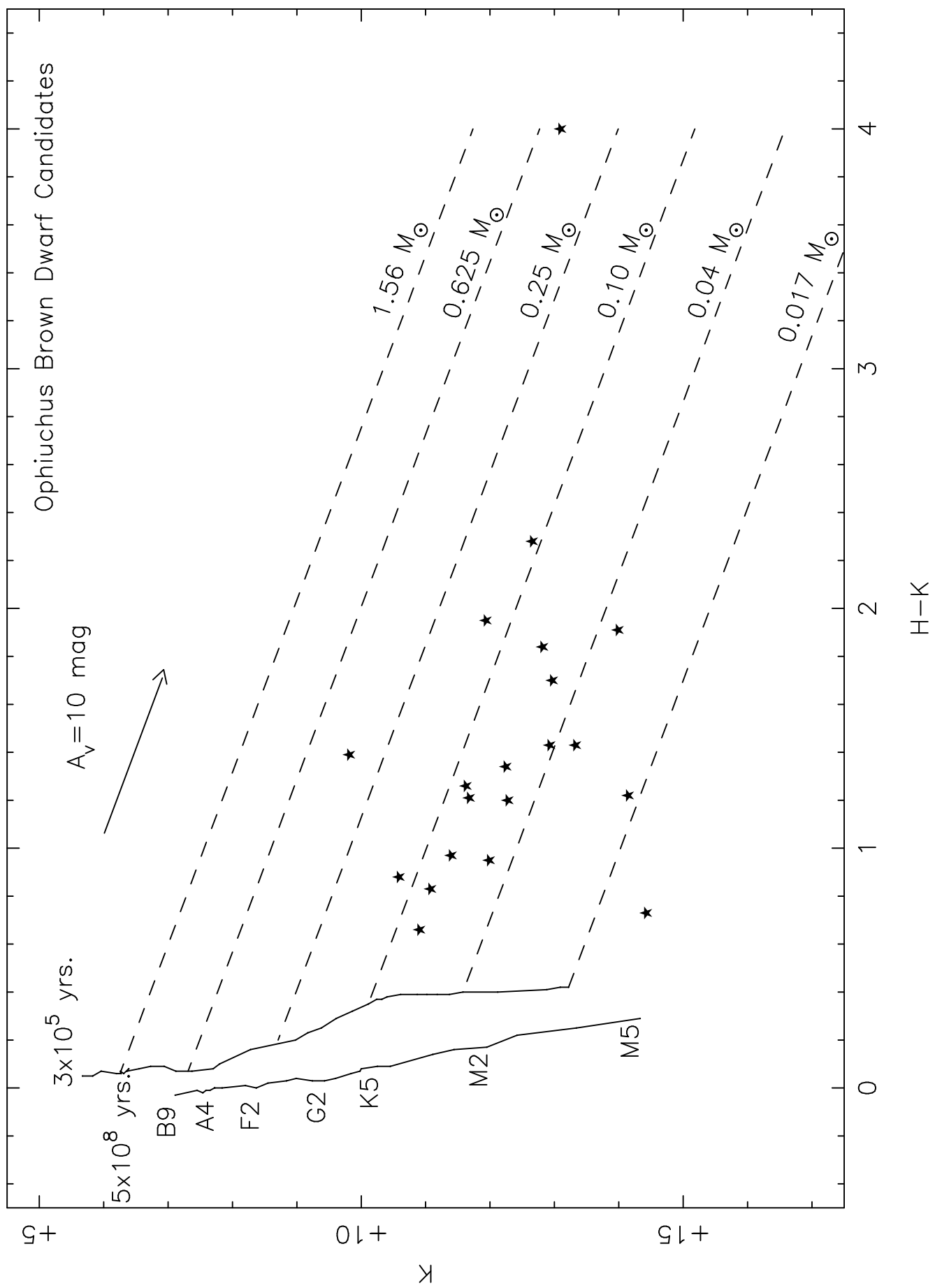


TABLE 1. Log of Brown Dwarf Candidate Observations

Object <sup>a</sup> 16 <sup>h</sup> , -24°	GY No. <sup>b</sup>	CRBR No. <sup>c</sup>	Other Names <sup>d</sup>	Date Observed (UT)	Int. Time (seconds)	Telluric Std.
2303.6-1805		1		1997 May 01	2880	HR 6070 (A0V)
2316.6-2131			BKLT 162618-242818	1997 Apr 30	1680	HR 6235 (A0IV/V)
2317.3-1925		14	SKS 1-10	1997 Apr 29	1440	HR 6235 (A0IV/V)
2317.5-1729		15	SKS 1-11	1996 Jun 06	960	HR 6066 (B9V)
2320.0-1915	5	21	SKS 1-13,ROXR1C14	1996 Jun 05	720	HR 6066 (B9V)
2320.8-1708	10	24	SKS 1-14	1996 Jun 04	1020	HR 6066 (B9V)
2320.8-1721	11	25	SKS 3-13,RR 3	1997 May 01	2280	HR 6070 (A0V)
2323.8-1640	31	34	SKS 3-15	1997 May 01	1440	HR 6070 (A0V)
2324.1-1619	30	36	SKS 3-16	1997 Jul 02	1680	HR 6070 (A0V)
2326.5-1958	37	37	VSSG 29,ROXR1C15	1996 Jun 04	1080	HR 6066 (B9V)
2330.1-1847	59	39	SKS 1-21	1997 Apr 29	840	HR 6235 (A0IV/V)
2331.1-1952	64	40		1997 Apr 30	960	HR 6235 (A0IV/V)
				1997 Jul 02	720	HR 6070 (A0V)
2337.5-1642	84		SKS 1-24	1997 Jul 01	1440	HR 6066 (B9V)
2341.4-1542	107			1997 May 01	1440	HR 6070 (A0V)
2347.1-3143	129		WL 18 <sup>e</sup>	1997 Jul 02	720	HR 6070 (A0V)
2355.3-2156	163	49		1997 Apr 30	1680	HR 5959 (A0Vs)
2404.5-2152	202	57	VSSG 31	1997 May 01	960	HR 5959 (A0Vs)
2408.6-2229	218	63	RR 9	1997 Jul 02	840	HR 6070 (A0V)
2436.9-3158	310		SKS 1-49	1997 Apr 30	1080	HR 6235 (A0IV/V)
2440.9-3210	326		SKS 1-52	1997 Apr 30	1200	HR 6235 (A0IV/V)

<sup>a</sup>Object RA (min, sec) and DEC (', '') in B1950.0.

<sup>b</sup>Greene & Young 1992.

<sup>c</sup>Comerón *et al.* 1993.

<sup>d</sup>Other sources names from infrared studies by Strom, Kepner, & Strom Tables 1 or 3 (SKS, 1993), Rieke & Rieke (RR, 1990), Vrba *et al.* (VSSG, 1975), Wilking & Lada (WL, 1983), Barsony *et al.* (BKLT, 1997), or the x-ray study by Casanova *et al.* (ROXR1, 1993).

<sup>e</sup>Star is reported to be a double by Barsony *et al.* 1989, with a separation of 3.5".

## M Dwarf Standards

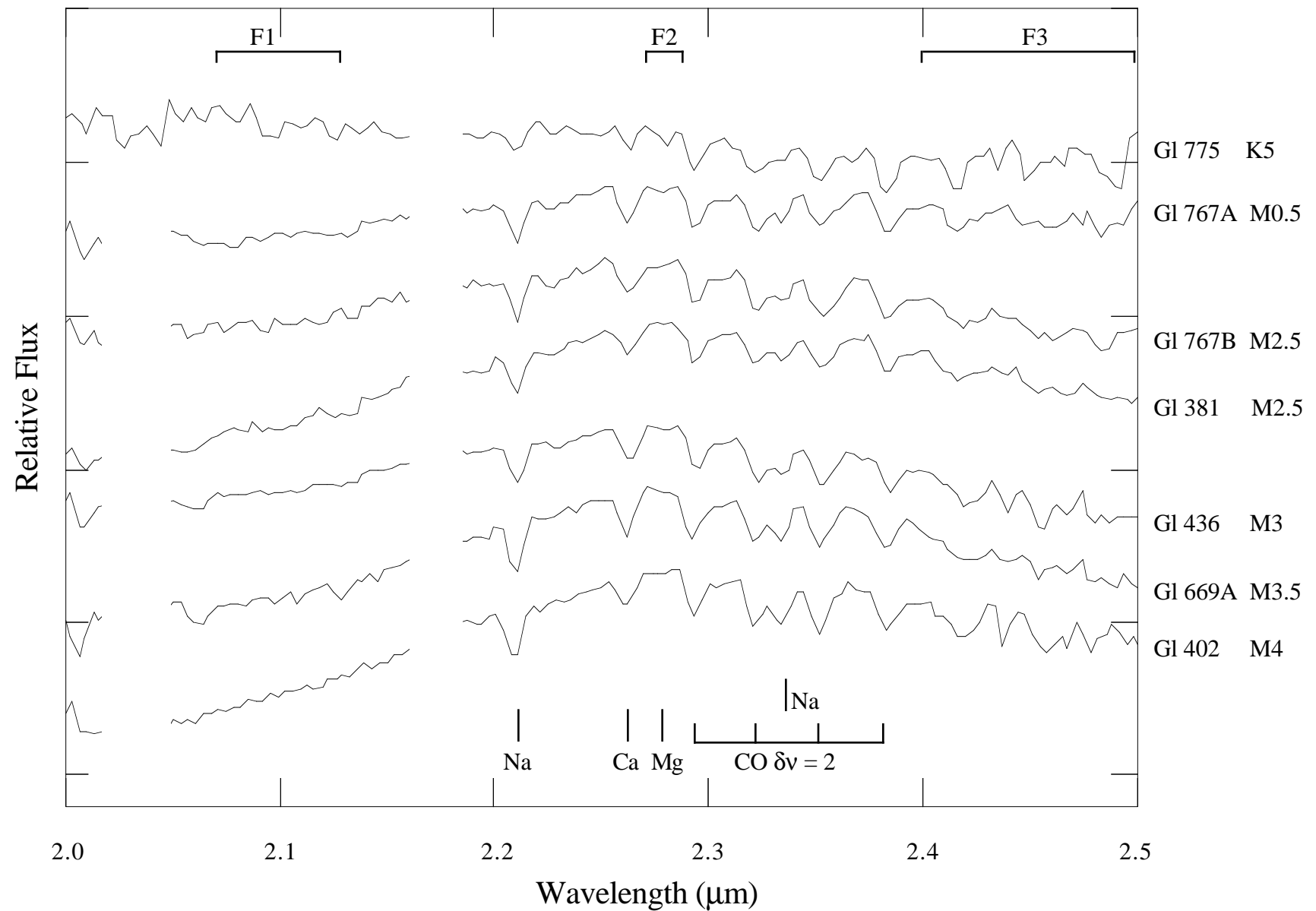


Fig. 2a

## M Dwarf Standards

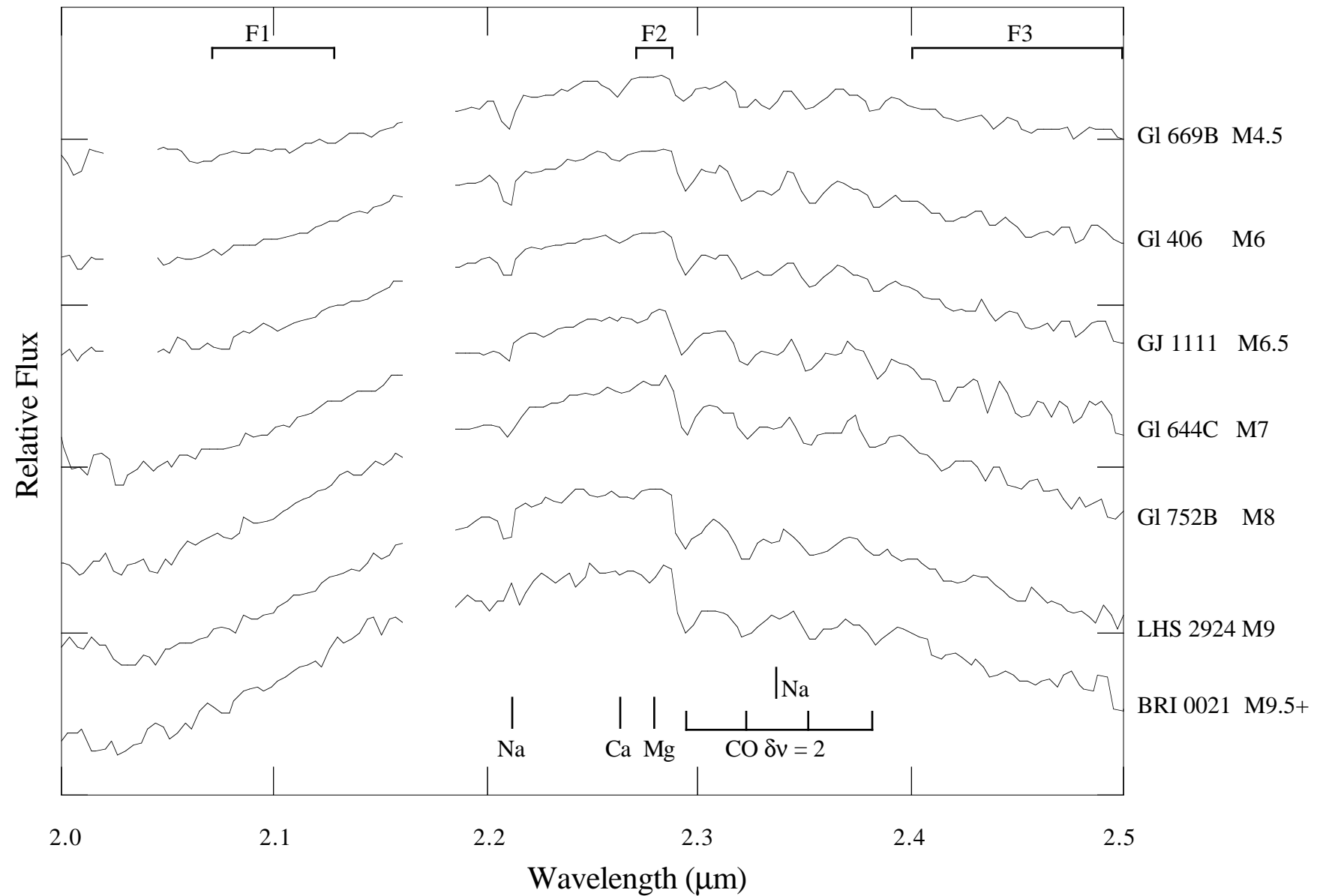


Fig. 2b

TABLE 2. Brown Dwarf Candidates in the  $\rho$  Oph Cloud

Object	Q <sup>a</sup>	Sp. Ty. ( $\pm 1.5$ )	log( $T_{eff}$ ) ( $\pm 0.035$ )	(J-H) (mag)	(H-K) (mag)	K <sup>b</sup> (mag)	A <sub>v</sub> <sup>c</sup> (mag)	log(L <sub>bol</sub> /L <sub>sun</sub> ) ( $\pm 0.16$ )	r <sub>k</sub> <sup>e</sup>	Comments
CRBR 14	0.51	M7.5	3.400	1.75	1.20	12.28	10	-1.58	0.12	
CRBR 15	0.64	M5	3.467	2.46	1.95	11.94	17	-1.32	0.64	mm cont. source <sup>f</sup>
GY 5	0.55	M7	3.414	1.13	0.66	10.91	4.5	-1.20	-0.03	poss. x-ray source <sup>g</sup>
GY 10	0.47	M8.5	3.371	2.16	1.34	12.25	14	-1.44	-0.01	no mm cont. <sup>h</sup>
GY 11	0.58	M6.5	3.428	1.15	1.22	14.15	4.8	-2.69	0.63	H <sub>2</sub> emission lines <sup>h</sup>
GY 31	0.63	M5.5	3.454	...	4.00	13.10	56 <sup>d</sup>	-0.15 <sup>d</sup>	...	radio cont. source <sup>i</sup>
GY 37	0.59	M6	3.441	1.31	0.95	11.99	6.3	-1.62	0.18	poss. x-ray source <sup>g</sup>
GY 59	0.61	M6	3.441	1.86	1.21	11.68	11	-1.29	0.11	
GY 64	0.49	M8	3.386	1.87	1.43	13.33	11	-2.07	0.28	
GY 84	0.61	M6	3.441	2.40	1.26	11.63	16	-0.99	-0.13	
GY 107	0.76	M3	3.513	2.02	0.97	11.40	13	-0.87	-0.11	poss. background giant
GY 163	0.79	M2.5	3.524	...	2.28	12.66	32 <sup>d</sup>	-0.75 <sup>d</sup>	...	
GY 202	0.53	M7	3.414	2.09	1.70	12.97	13	-1.90	0.50	
GY 310	0.47	M8.5	3.371	1.29	0.83	11.08	5.7	-1.26	-0.01	
GY 326	0.71	M4	3.490	1.78	0.88	10.59	11	-0.70	-0.09	

<sup>a</sup>Water vapor index Q (see eqn. 1, Sec. 3.1).

<sup>b</sup>All photometry taken from Barsony *et al.* (1997) except that for GY31 taken from Comerón *et al.* (1993).

<sup>c</sup>Visual extinction A<sub>v</sub> = 9.09 × [(J - H)<sub>obs</sub> - (J - H)<sub>0</sub>] except where noted.

<sup>d</sup>No J photometry is available so A<sub>v</sub> = 15.4 × [(H - K)<sub>obs</sub> - (H - K)<sub>0</sub>], and L<sub>bol</sub> is estimated from the absolute K magnitude plus the bolometric correction at K.

<sup>e</sup>Excess emission at  $\lambda=2.2$   $\mu$ m, r<sub>k</sub> = F<sub>Ke</sub>/F<sub>K\*</sub>, assuming no excess emission at H. Estimates are lower limits to the true values. See Sec. 3.2.2 for discussion.

<sup>f</sup>Millimeter continuum source with S<sub>1.3mm</sub>=40 mJy (Motte, André, & Neri 1998).

<sup>g</sup>Candidate x-ray sources from Table 3 of Casanova *et al.* 1993.

<sup>h</sup>Subtraction of background emission reduces level of millimeter continuum emission at  $\lambda=1.3$  mm to <10 mJy (Motte, André, & Neri 1998).

<sup>i</sup>Highly variable radio emission is observed at  $\lambda=6$  cm by André (priv. comm.), probably arising from nonthermal geosynchrotron emission from a peristellar magnetosphere.

### Dwarf Star Spectral Standards (KHM91)

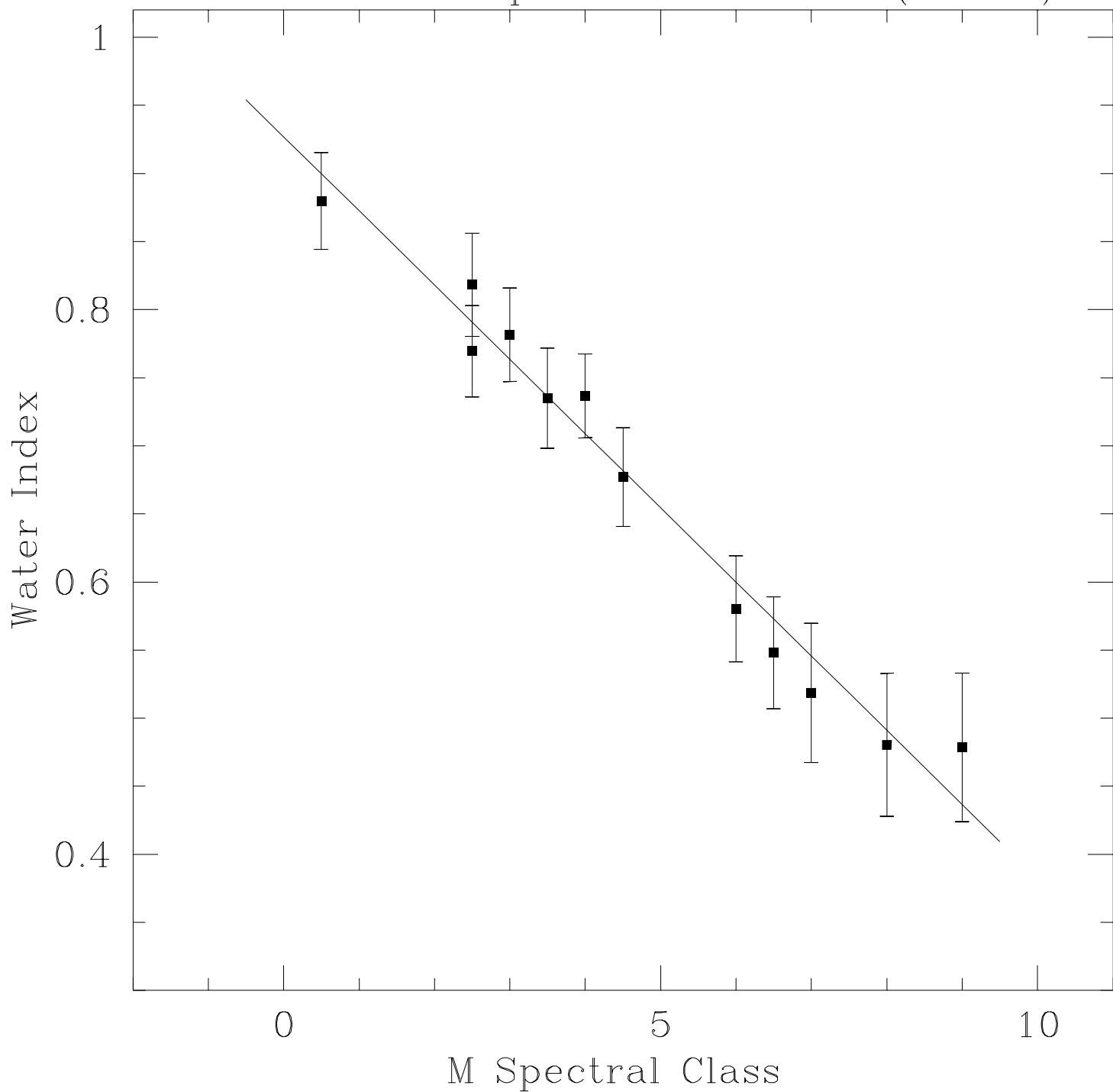


TABLE 3. Masses &amp; Ages for Brown Dwarf Candidates

Object	DM 98 <sup>a</sup>		Burrows <i>et al.</i> 97 <sup>b</sup>		Comments
	Mass( $M_{\odot}$ )	Age( $10^6$ yrs.)	Mass( $M_{\odot}$ )	Age( $10^6$ yrs.)	
CRBR 14	0.03	<0.1	0.03	0.2	
CRBR 15	<0.12	<3	<0.09	<3.0	veiled
GY 5	0.06	0.2	0.05	<0.1	
GY 10	0.03:	<0.1	0.02	<0.1	
GY 11	<0.03	<10	<0.05	<60	veiled
GY 31	0.10	<0.1	>0.24	<0.1	
GY 37	0.06	2.0	0.05	1.0	
GY 59	0.08	1.0	0.06	0.3	
GY 64	0.02:	<0.1	0.02	0.5	veiled
GY 84	0.10	0.3	0.08	0.2	
GY 107	0.20	2.0	>0.24	3.0	poss. background giant (c)
GY 163	0.22	2.0	>0.24	3.0	(c)
GY 202	<0.03	<0.3	<0.035	<1.0	veiled
GY 310	0.04:	<0.1	0.03	<0.1	
GY 326	0.15	0.3	0.20	2.0	(c)

<sup>a</sup>Masses and ages estimated using models of D'Antona & Mazzitelli 1998. Values followed by a ":" are poorly defined by the evolutionary tracks/isochrones.

<sup>b</sup>Masses and ages estimated using models of Burrows *et al.* 1997. Values followed by a ":" are poorly defined by the evolutionary tracks/isochrones.

<sup>c</sup>Uncertainties in mass  $> 0.04 M_{\odot}$ .

## Brown Dwarf Candidates

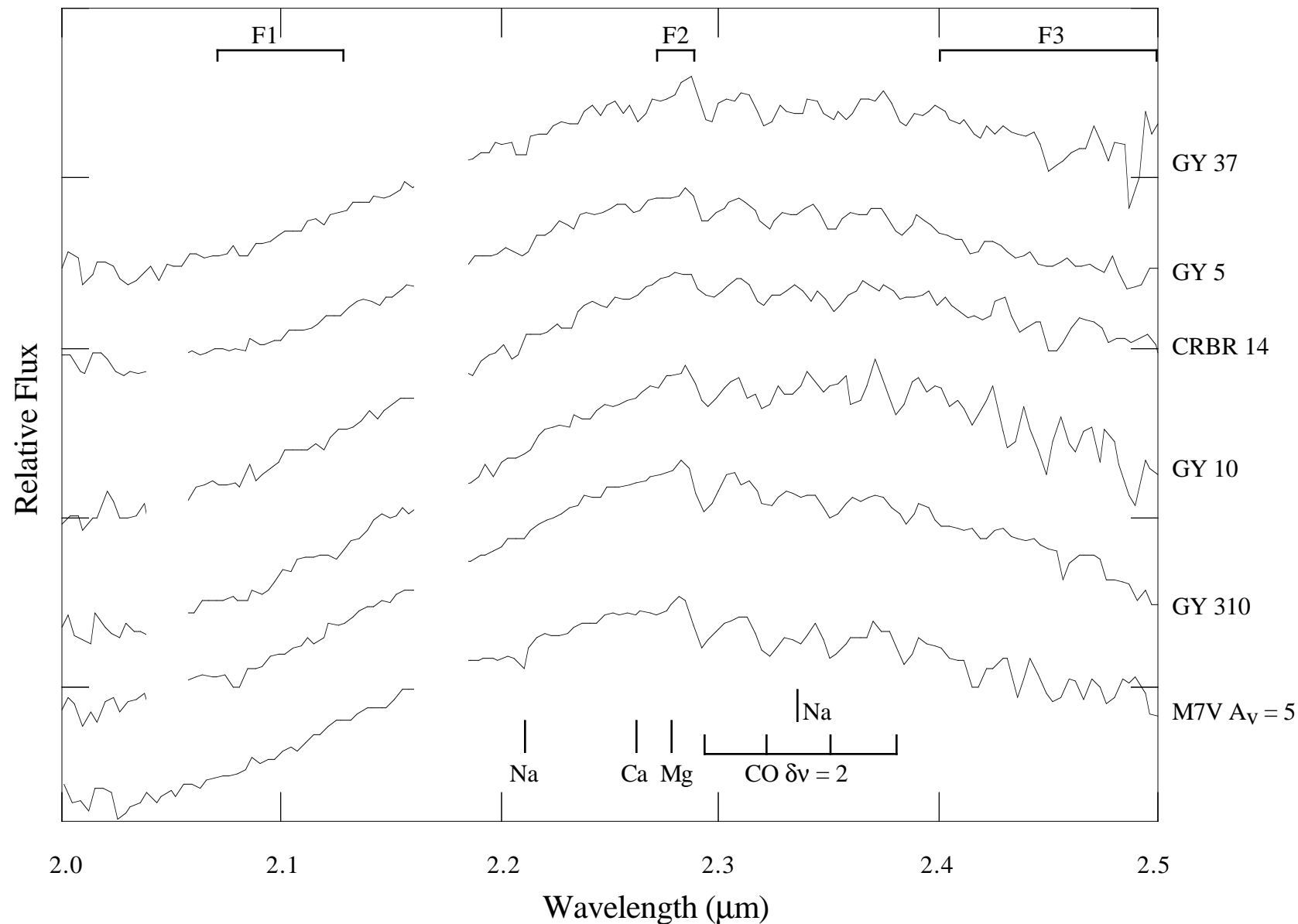


Fig. 4a

## Brown Dwarf Candidates

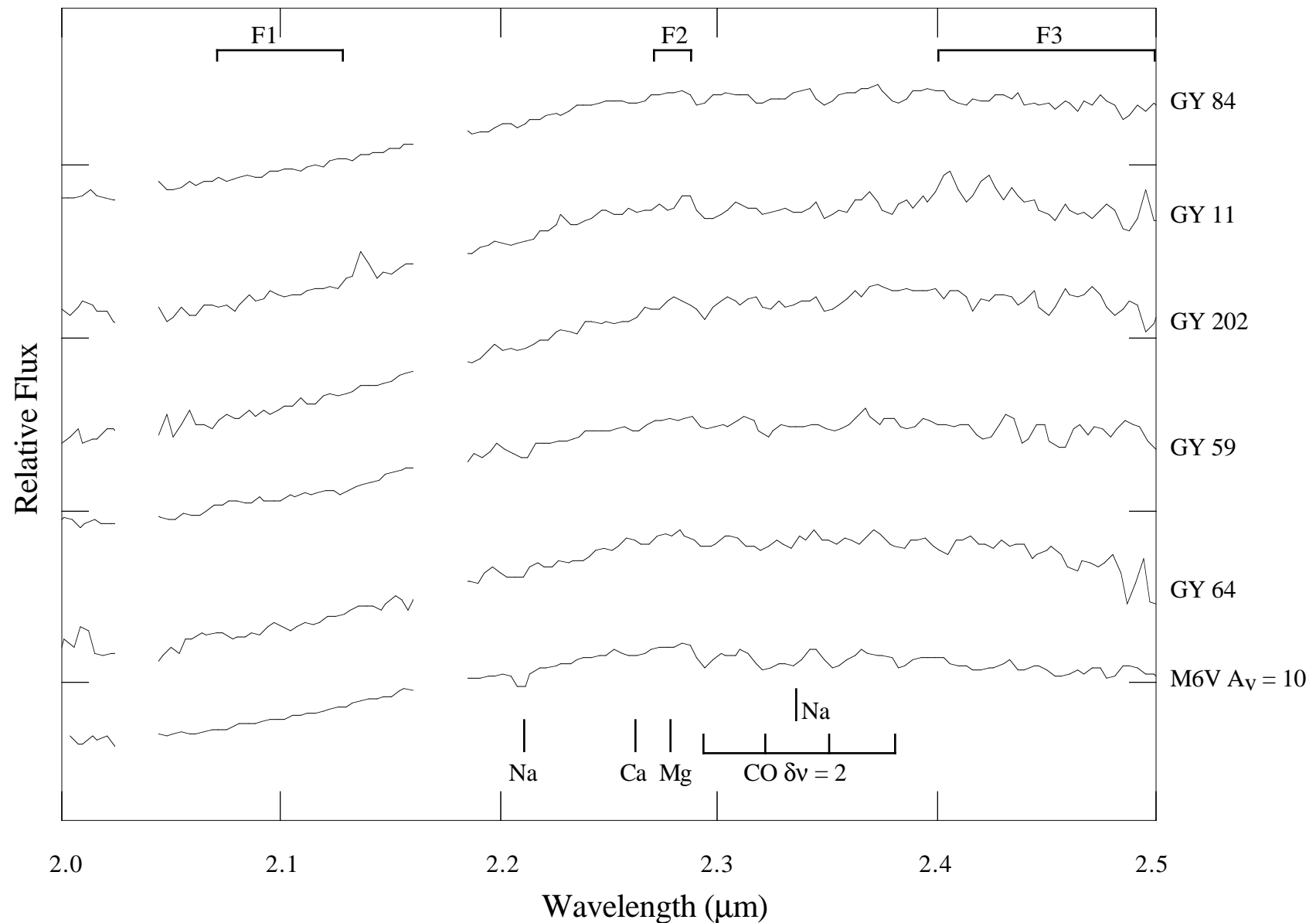


Fig. 4b

TABLE 4. Temperatures and Colors for M Dwarfs

Star	Sp. Ty.	$T_{eff}$	$(J - H)_0$	$(H - K)_0$	$BC_J$	$BC_K$
Gl 411	M2 V	3420	0.54	0.20	1.84	2.58
Gl 569A	M3 V	3320	...	...	...	...
Gl 388	M3 V	3230	0.64	0.21	1.83	2.68
Gl 748AB	M3.5 V	...	0.53	0.24	1.93	2.70
Gl 729	M3.5 V	...	0.54	0.28	1.97	2.79
Gl 876	M3.5 V	...	0.60	0.26	1.96	2.82
Gl 896A	M3.5 V	...	0.58	0.22	1.87	2.67
Gl 447	M4 V	...	0.58	0.28	1.92	2.78
Gl 831	M4.5 V	...	0.59	0.28	2.00	2.87
Gl 268	M4.5 V	...	0.62	0.28	1.90	2.80
Gl 866AB	M5 V	...	0.59	0.34	2.05	2.98
GJ 1002	M5.5 V	...	0.55	0.33	1.96	2.84
Gl 65AB	M5.5 V	...	0.57	0.34	1.99	2.90
Gl 406	M6 V	2670	0.62	0.36	2.09	3.07
GJ 1111	M6.5	2700	0.58	0.36	2.05	2.99
Gl 644C	M7 V	...	0.58	0.37	2.17	3.12
Gl 752B	M8 V	2510	0.66	0.44	2.03	3.13
Gl 569B	M8.5	2360	...	...	...	...
LHS 2924	M9 V	2220	0.67	0.50	2.05	3.22
LHS 2065	M9 V	...	0.75	0.51	1.93	3.19

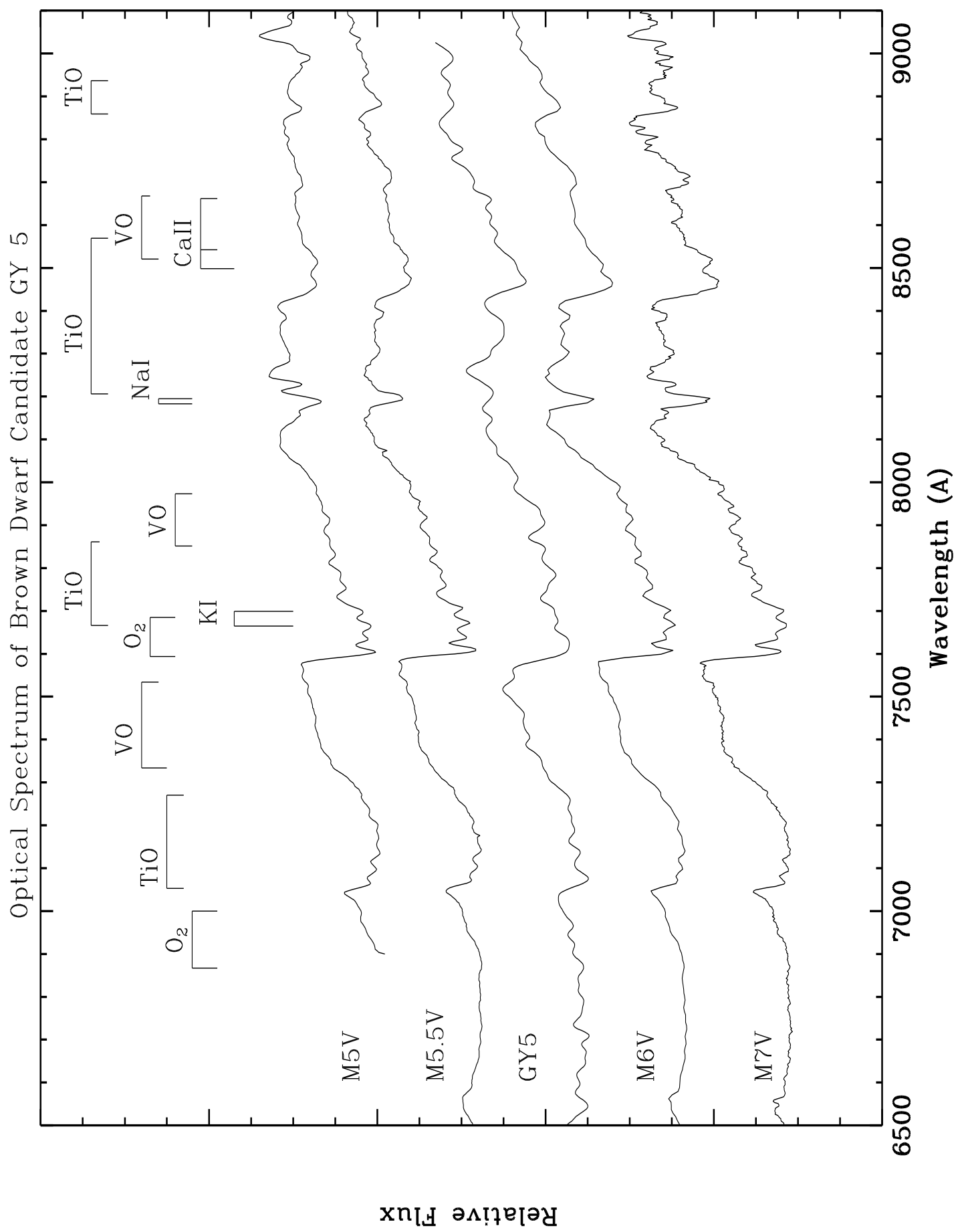
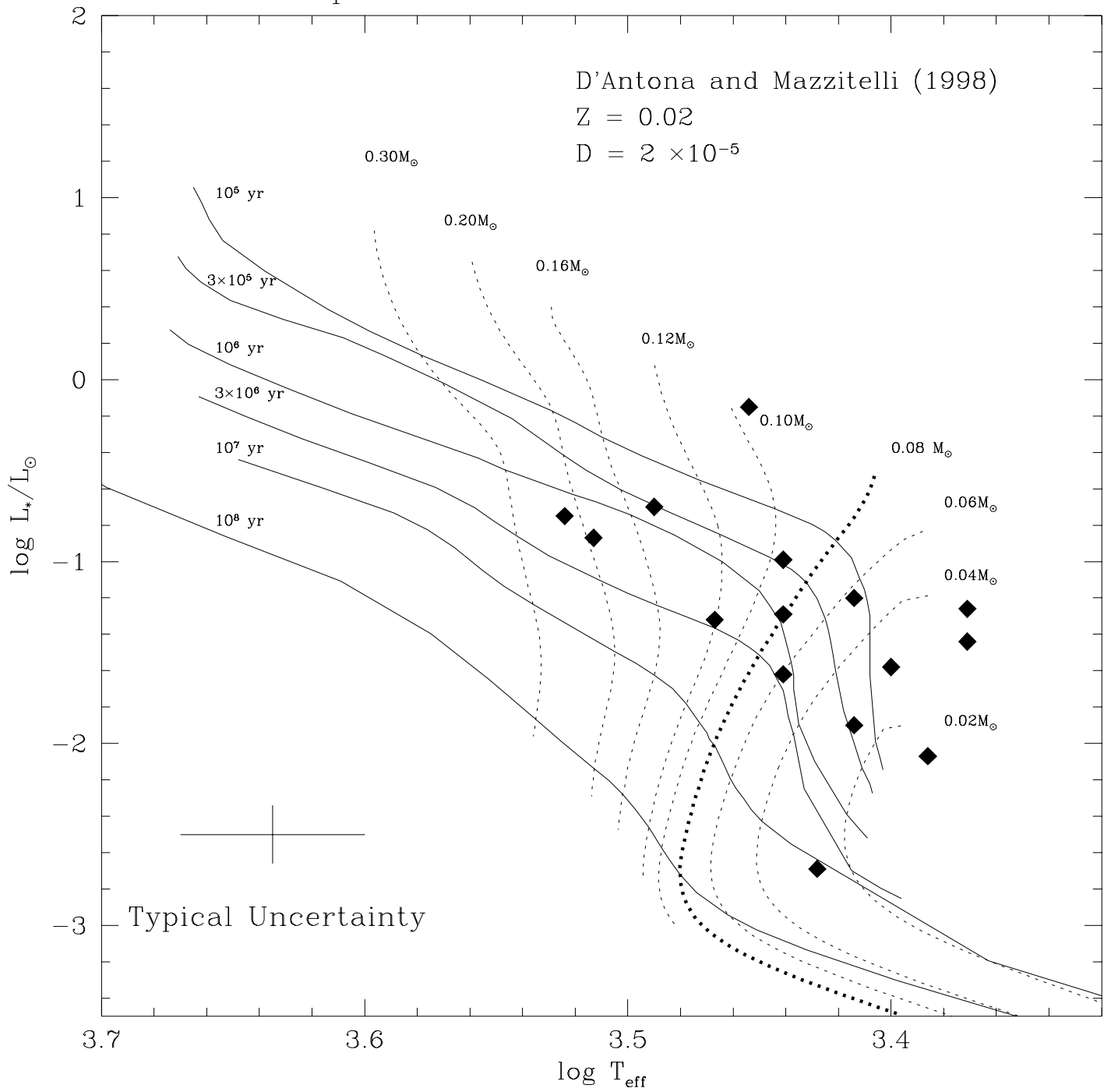


TABLE 5. Adopted Temperature Scale and Colors

Sp. Ty.	$T_{eff}$	$(J - H)_0$	$(H - K)_0$	$BC_J$	$BC_K$
M2 V	3426	0.54	0.18	1.79	2.61
M2.5 V	3343	0.55	0.21	1.84	2.66
M3 V	3260	0.56	0.23	1.88	2.70
M3.5 V	3177	0.57	0.25	1.92	2.75
M4 V	3094	0.58	0.27	1.96	2.79
M4.5 V	3011	0.59	0.29	1.99	2.84
M5 V	2928	0.60	0.31	2.01	2.88
M5.5 V	2845	0.61	0.34	2.03	2.93
M6 V	2762	0.62	0.36	2.04	2.97
M6.5 V	2679	0.62	0.38	2.05	3.02
M7 V	2596	0.63	0.40	2.06	3.06
M7.5 V	2513	0.64	0.42	2.05	3.11
M8 V	2430	0.65	0.45	2.05	3.15
M8.5 V	2348	0.66	0.47	2.03	3.19
M9 V	2265	0.67	0.49	2.02	3.24

## Ophiuchus Brown Dwarf Candidates



## Ophiuchus Brown Dwarf Candidates

